CORROSION SCIENCE AND TECHNOLOGY, Vol.23, No.1(2024), pp.33~40 pISSN 1598-6462 / eISSN 2288-6524
[Research Paper] DOI: https://doi.org/10.14773/cst.2024.23.1.33

The Effect of Mo Addition on Oxygen Vacancies in the Oxide Scale of Ferritic Stainless Steel for SOFC Interconnects

Dae Won Yun†, Hi Won Jeong, Seong Moon Seo, Hyung Soo Lee and Young Soo Yoo

Korea Institute of Materials Science, 797 Changwondaero, Changwon, Gyungnam 51580, South Korea
(Received November 13, 2023; Revised November 28, 2023; Accepted November 28, 2023)

The concentration and diffusion coefficient of oxide ion vacancies in the oxide scale formed on Fe-22Cr-0.5Mn ferritic stainless steel with and without molybdenum (Mo) was measured at 800°C by the electrochemical polarization method. After pre-oxidation for 100 h in ambient air at 800 °C, the oxide scale on one side was completely removed with sandpaper. A YSZ plate was placed on the side where the oxide scale remained. Platinum (Pt) meshes were attached on the top of the YSZ plate and the side where the oxide scale was removed. Changes in electrical current were measured after applying an electrical potential through Pt wires welded to the Pt meshes. The results were interpreted by solving the diffusion equation. The diffusion coefficient and concentration of oxide ion vacancy decreased by 30% and 70% in the specimen with Mo, respectively, compared to the specimen without Mo. The oxide ion vacancy concentration of chromia decreased due to the addition of Mo.

Keywords: *Stainless steel, Solid oxide fuel cell, Interconnect, Molybdenum, Oxidation*

1. Introduction

The interconnect is one of key components in planar-type SOFCs. The interconnect provides gas channels and electric connections between unit cells, and acts as a physical barrier that separates fuel and air. Ferritic stainless steels are used as an interconnect material for planar-type SOFCs considering cost, formability, coefficient for thermal expansion and so on [1]. However, there are decisive problems in using ferritic stainless steels as an interconnect material, which is major degradation mechanism for SOFCs. In an oxidizing atmosphere, oxide scales forms on the steel surface, which leads to increase in the area specific resistance (ASR) of interconnects. Volatile Cr species evaporated from Cr-containing oxide scale migrate to the cathode of SOFC, and deteriorate catalytic activity of the cathode. This phenomenon is well-known as Cr poisoning [2-4].

Many researchers have put efforts into development of new alloys [5-13] and coatings [14-16] to mitigate these problems. Although recent researches have mainly focused on coating development, alloy development is also important to secure a long lifespan and to ensure stability of a SOFC system in case of local coating failure. Related to the development of new alloys, studies on the effects of various alloy elements such as Mo, W, Nb, Ti and Si have been reported in the literature [5-13].

In our previous studies, the addition of 0.1 to 2 wt% Mo improved the oxidation resistance and electric conductivity of Fe-22Cr-0.5Mn ferritic stainless steel [5]. The beneficial effect of Mo addition was also confirmed in button cell tests [6]. Although the Pt marker test results and the activation energy calculation results for electrical conductivity suggested that Mo altered ionic defects of chromia scale [5], direct and quantitative analysis was not conducted. There are studies reported that the addition of Mo improves corrosion resistance of stainless steels by affecting the passive film in an aqueous corrosion environment [17-19]. However, the effect of Mo addition on the defect structure of the oxide scale at high temperatures is rarely reported in the literature. In this study, the effect of Mo on oxide ion vacancies in chromia was quantitatively investigated by using an electrochemical polarization method and diffusion equations.

2. Materials and Methods

Ferritic stainless steels with Mo (MoP1, Fe-22Cr-

†Corresponding author: dwyun@kims.re.kr
Dae Won Yun: Senior Researcher, Hi Won Jeong: Principal Researcher, Seong Moon Seo: Principal Researcher, Hyung Soo Lee: Senior Researcher, Young Soo Yoo: Principal Researcher

0.5Mn) and without Mo (Base, Fe-22Cr-0.5Mn) were used in the experiment. Detailed descriptions of sample preparation methods and compositional analysis results are presented in previous studies [5]. Each specimen was cut into rectangular shape with 20 × 20 × 5 mm in size and all surfaces were ground up to P4000 grade with sandpapers. The specimen was rinsed with ethanol and acetone to remove any surface contaminants. The pre-oxidation was conducted for 100 h in ambient air at 800 ºC. To prevent any damage on the oxide scale due to thermal shock, the rate of temperature change during heating and cooling was controlled to less than 5 °C per minute.

After the pre-oxidation, the oxide scale on one side was completely removed with sandpaper. Then, a Pt mesh was attached on the side without oxide scale after applying Pt paste. On the side where the oxide scale remained, a Pyrex glass seal was applied along the edge to a width of 5 mm, and 500 μm thick 8YSZ with 20 × 20 mm in size was placed on top of the specimen. Then, a Pt mesh was attached on the top of the 8YSZ plate after applying Pt paste. Two Pt wires were welded to both Pt meshes and used to apply voltage and to measure current, respectively. The schematic diagram containing information about the oxygen partial pressure at each interface and the potential between the interfaces is shown in Fig. 1.

In Fig. 1, interfaces I, II and III are interfaces between air and YSZ, YSZ and oxide scale, and oxide scale and metal substrate, respectively. $P^{I}_{O_2}$, $P^{II}_{O_2}$, and $P^{III}_{O_2}$ are the equilibrium oxygen partial pressures at each interface. $E^{I\text{-}II}$ is electrical potential introduced by the difference in oxygen partial pressure between interface I and interface II. $E^{II\text{-}III}$ is electrical potential introduced by the difference in oxygen partial pressure across the oxide scale (between interface II and interface III). Since the chromia scale is almost pure electric conductor at 800 ºC [20], an internal short circuit is formed and $E^{II\text{-}III}$ cannot be measured in an external circuit. The potential measured in an external circuit can be expressed as the following equation.

$$V = t_{ion}(YSZ) \times E^{I-II} + t_{ion}(scale) \times E^{I-II}$$

Where V is potential measured in an external circuit, and t_{ion} is ionic transport number.

The ionic transport number of YSZ ($t_{ion}(YSZ)$), which is regarded as a pure oxide ion conductor, is nearly one. And that of chromia ($t_{ion}(scale)$) is nearly zero [20]. Therefore, the potential measured in an external circuit (V) can be considered the same as the electrical potential across YSZ ($E^{I\text{-}II}$).

Fig. 2 is a schematic diagram showing the change in concentration of oxide ion vacancies inside the oxide scale before and after an external potential is applied. The electrical potential applied by the external circuit is applied to YSZ, which result in a change in the oxygen partial pressure at the interface between the YSZ and the oxide scale (interface II). Then, the equilibrium concentration of oxide ion vacancies at interface II of the oxide scale changes. The concentration of oxide ion vacancies in the oxide scale changes by diffusion until a new steady state is reached. Since oxide ion vacancy has +2 charge, this change in the concentration of oxide ion vacancies can be measured as a current through the external circuit. In other words, after applying an electrical potential through an external circuit, the change in current can be measured and analyzed to obtain information about the concentration and diffusion coefficient of oxide ion vacancies in the oxide scale.

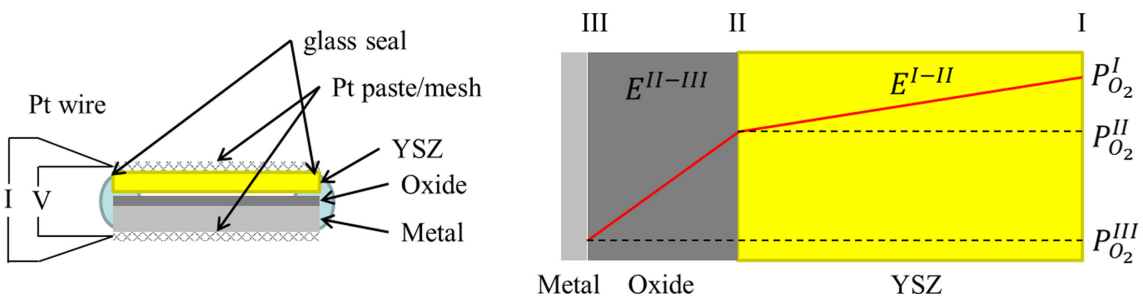

Fig. 1. The schematic diagram for an electrochemical polarization method and information about the oxygen partial pressure at each interface and the potential

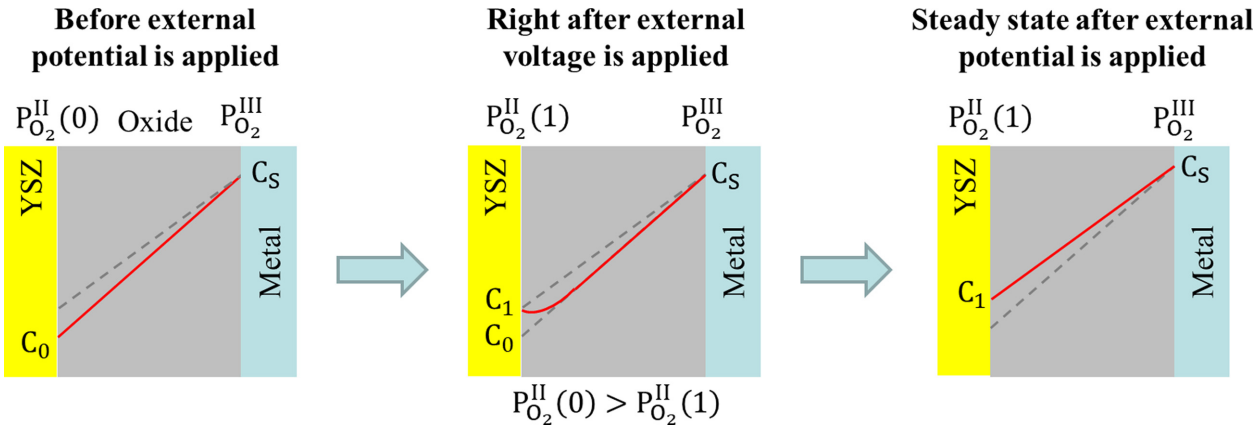

Fig. 2 Simple representation of oxide ion vacancy measurement by electrochemical method

3. Results and Discussion

3.1 Solution for Diffusion Equations

The concentration of oxide ion vacancies is a function of time (t) and position (x) along the thickness of the oxide scale. This function can be separated into sum of two functions with variables into a time-related part (u) and a non-time-related part (V), respectively.

$$C(x,t) = u(x,t) + V(x)$$

Because the concentration at both boundaries is fixed regardless of time, $u(x,t)$ can be expressed as the following general solution.

$$u(x,t) = \sum_{n=1}^{\infty} B_n \sin\lambda_n x \cdot \exp(-\lambda_n^2 \tilde{D} t) \quad \left(\lambda_n = \frac{n\pi}{L}\right)$$

Where $\tilde{D}$ is diffusion coefficient of oxide ion vacancy and L is the thickness of the oxide scale.

Function $u(x,t)$ converges to zero when time goes to infinity. Therefore, $V(x)$ is equal to the straight line between C_1 and C_s, which are in a steady state after external potential is applied, and can be expressed as follows.

$$V(x) = \frac{(C_1 - C_s)}{L} x + C_s$$

When $t = 0$, the concentration profile is a straight line between C_0 and C_s, so the following equation holds.

$$C(x,0)$$

$$= \sum_{n=1}^{\infty} B_n \sin\lambda_n x \cdot \exp(-\lambda_n^2 \tilde{D} t) + \frac{(C_1 - C_s)}{L} x + C_s$$

$$= \frac{(C_0 - C_s)}{L} x + C_s$$

$$\sum_{n=1}^{\infty} B_n \sin\lambda_n x \cdot \exp(-\lambda_n^2 \tilde{D} t)$$

$$= \frac{(C_0 - C_1)}{L} x = \frac{\Delta C}{L} x$$

By solving this equation, B_n and $C(x,t)$ can be expressed as follows.

$$B_n = \frac{2}{L}\int_0^L \frac{\Delta C}{L} x \sin\frac{n\pi}{L} x\, dx = (-1)^{n+1}\frac{2\Delta C}{n\pi}$$

$$C(x,t) = \frac{2\Delta C}{\pi}\sum_{n=1}^{\infty}\frac{(-1)^{n+1}}{n}\sin\frac{n\pi}{L}x \cdot \exp\left(-\frac{n^2\pi^2\tilde{D}}{L^2}t\right) + \frac{(C_1 - C_S)}{L}x$$

The electrical current is equal to the change in total charge (Q) over time, and the total charge can be obtained by integrating function $C(x,t)$ in the thickness direction.

$$I(t) = \frac{dQ(t)}{dt} = neA\frac{d}{dt}\left(\int_0^L C(x,t)dx\right)$$

$$Q_t = \frac{1}{2}\Delta CLneA$$

Where e = electron charge, n = valence of charge carrier, A = area and n = 2 in the case of oxide ion vacancy.

These integral and differential equations can be solved as follows.

$$I(t) = \frac{2Q}{\Delta CL}\frac{d}{dt}\left(\int_0^L C(x,t)dx\right)$$

$$= \frac{4Q}{\pi L}\frac{d}{dt}\left(\sum_{n=1}^{\infty}\frac{(-1)^{n+1}}{n}\int_0^L \sin\frac{n\pi}{L}x\,dx \cdot \exp\left(-\frac{n^2\pi^2\tilde{D}t}{L^2}\right) + \frac{\pi}{2\Delta C}\frac{(C_1 - C_S)}{L}x\,dx\right)$$

$$= \frac{4Q}{\pi^2}\frac{d}{dt}\left(\sum_{n=1}^{\infty}\frac{(-1)^{n+1}}{n^2}(1-\cos n\pi) \cdot \exp\left(-\frac{n^2\pi^2\tilde{D}t}{L^2}\right) + \frac{\pi^2}{4\Delta C}(C_1 - C_S)\right)$$

$$= -\frac{8Q\tilde{D}}{L^2}\sum_{n=1}^{\infty}\exp\left(-\frac{(2j-1)^2\pi^2\tilde{D}t}{L^2}\right)$$

Under the condition of $t \gg L^2/\pi^2\tilde{D}$, terms where j is two or more can be ignored and the electrical current can be expressed briefly as follows.

$$|I(t)| \approx \frac{8Q\tilde{D}}{L^2}\exp\left(-\frac{\pi^2\tilde{D}t}{L^2}\right) \quad (t \gg L/\pi^2\tilde{D})$$

$$\ln|I(t)| \approx \ln\frac{8Q\tilde{D}}{L^2} - \frac{\pi^2\tilde{D}t}{L^2} \quad (t \gg L/\pi^2\tilde{D})$$

Therefore, $\tilde{D}$ can be calculated by plotting logarithm of the electrical current over time, and the changes in the concentration of oxide ion vacancies (ΔC), can be obtained through the amount of total charge (Q_t).

3.2 Electrochemical Polarization Method

As explained in section 2, external electrical potential are applied to YSZ. $P_{O_2}^{I}$ is ambient air, so it is fixed at 0.21 atm (Fig. 1). Therefore, $P_{O_2}^{II}$ is determined by the following equation depending on the applied electrical potential (E). Alternatively, E can be determined to adjust the oxygen partial pressure of interface II to a certain value.

$$E = \frac{RT}{4F}\ln\frac{P_{O_2}^{I}}{P_{O_2}^{II}}$$

$$P_{O_2}^{I} = 0.21 atm$$

In order to obtain information about the total amount of oxide ion vacancies affecting the diffusion process, the potential was determined to set the concentration gradient of oxide ion vacancies to almost zero. Since the

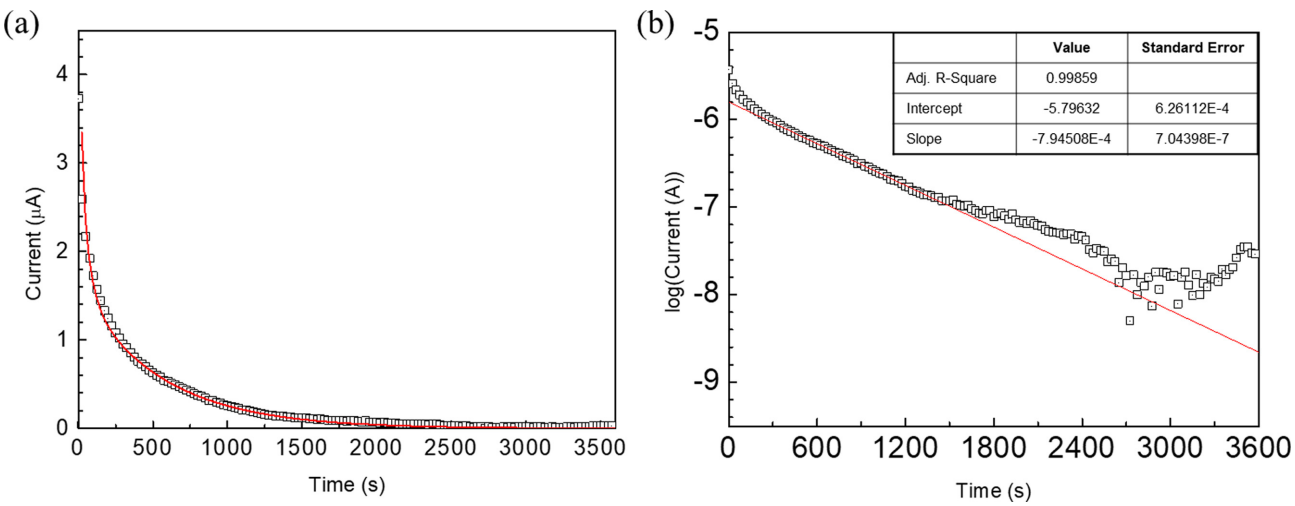

Fig. 3. Electrochemical test results of Base (Fe-22Cr-0.5Mn): (a) current versus time and fitted curve (b) log current versus time and fitted line

equilibrium oxygen partial pressure between chromia and Fe-22Cr at 800 ºC is about 4.1×10^{-27} atm, the electrical potential (E) should be about 1.4 V. Although there is a spinel on the outermost part of the oxide scale, both specimens form chromia as the major oxidation product and have the same bi- layer structure of chromia and Cr-Mn spinel [5]. Therefore, relative comparisons are meaningful. Therefore, the values measured by this method can somewhat differ from the actual values, but it is meaningful for a comparative study.

Fig. 3 is the result of the electrochemical polarization experiment on the Base specimen and fitted curve by the equations in section 3.1. At the initial stage, the current value decreased rapidly as the concentration gradient across the oxide scale decreased (Fig. 3a). To obtain the diffusion coefficient and total charge, the current was re-plotted on a logarithmic scale as shown in Fig. 3b. At the initial stage where the $t > L^2/\pi^2\tilde{D}$ condition was not satisfied, there was some deviation from linear behavior. However, it can be seen that the $t > L^2/\pi^2\tilde{D}$ condition was satisfied and linear behavior appears after a certain period of time. If the slope is s, the diffusion coefficient can be obtained by the following equation. The thickness of the oxide layer (L) was taken from the previous study [5]. The total charge and $L^2/\pi^2\tilde{D}$ were also calculated from the experimental data.

$$\tilde{D} = -\frac{s \times 2.303 \times L^2}{\pi^2}$$

$$= -\frac{-7.95 \times 10^{-4} \times 2.303 \times (0.98 \times 10^{-4})^2}{\pi^2}$$

$$= 1.78 \times 10^{-12} \text{ cm}^2/\text{s}$$

$$Q_t = 1.07 \times 10^{-3} \text{ C}$$

$$L^2/\pi^2\tilde{D} = 547 \text{ s}$$

The $L^2/\pi^2\tilde{D}$ value calculated from the diffusion coefficient is 547 s, which is very close to the time when linear behaviour began to appear in Fig. 3b. The change in oxide ion vacancy concentration at interface II (ΔC) can be calculated using the total charge as follows.

$$\Delta C = \frac{2Q_t}{LneA} = \frac{Q_t}{Le} = \frac{1.07 \times 10^{-3}}{0.98 \times 10^{-4} \times 1.602 \times 10^{-19}}$$

$$= 6.82 \times 10^{19} \text{ cm}^{-3}$$

Fig. 4 is the result of the electrochemical polarization experiment on the MoP1 specimen and fitted curve by the equations in section 3.1. Similar trends to the Base specimen were observed in the MoP1 specimen. In the same way as in the previous case, diffusion coefficient, the total charge and the change in oxide ion vacancy concentration were calculated as follows.

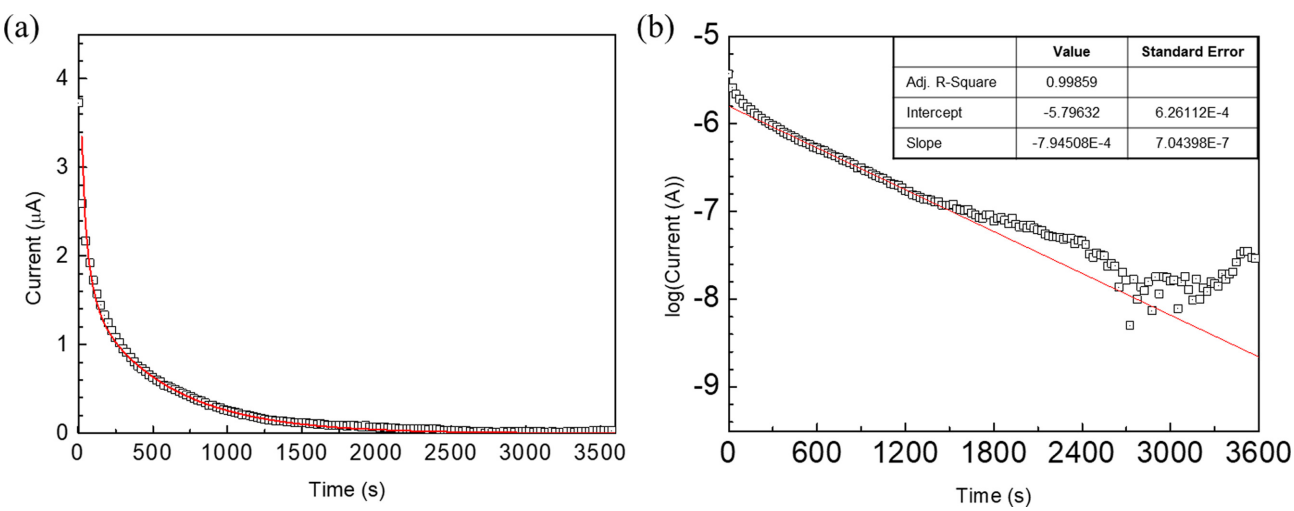

Fig. 4. Electrochemical test results of MoP1 (Fe-22Cr-0.5Mn-0.1Mo): (a) current versus time and fitted curve (b) log current versus time and fitted line

$$\tilde{D} = -\frac{s \times 2.303 \times L^2}{\pi^2}$$

$$= -\frac{-1.82 \times 10^{-3} \times 2.303 \times (0.54 \times 10^{-4})^2}{\pi^2}$$

$$= 1.24 \times 10^{-12} \text{ cm}^2/\text{s}$$

$$Q_t = 1.8 \times 10^{-4} \ C$$

$$L^2/\pi^2\tilde{D} = 238 \text{ s}$$

$$\Delta C = \frac{2Qt}{LneA} = \frac{Q_t}{Le}$$

$$= \frac{1.8 \times 10^{-4}}{0.54 \times 10^{-4} \times 1.602 \times 10^{-19}} = 2.08 \times 10^{19} \text{ cm}^{-3}$$

Firstly, the measured values w ere compared w ith those in the literature to ensure that they were within a reasonable range. No literature could be found on the concentration of oxide ion defects in chromia at 800 ºC. However, considering that the Cr defect concentration of chromia is 2.5×10^{19} cm^{-3} at 700 ºC [20], the concentration of oxide ion vancancy measured in this study seems to be within a reasonable range. The diffusion coefficient of oxygen in chromia reported in the literature is at the level of 10^{-13} cm^2/s based on the grain boundary diffusion [21-24], but it can increase by more than one order of magnitude depending on the impurity within the chromia [25]. Therefore, the diffusion coefficient of oxide ion vacancy obtained in this study can be considered a meaningful value.

Compared to the Base specimen, the diffusion coefficient and concentration of oxide ion vacancy decreased by 30% and 70% in the MoP1 specimen, respectively. The oxide ion vacancy concentration of chromia appears to have decreased due to the addition of Mo by the following reaction suggested in the previous study [5].

$$2MoO_2 \overset{Cr_2O_3}{\rightarrow} 2Mo_{Cr} + 3O_O^X + \frac{1}{2}O_2 + 2e'$$

$$\frac{1}{2}O_2 + V_{\ddot{O}} + 2e' \rightarrow O_O^X$$

To ensure whether the addition of 0.1 wt% Mo could cause this change in the concentration of oxide ion vacancy, the ratio of the measured concentration values a mong the total oxygen sites in chromia was calculated. The density of chromia at 800 ºC considering thermal expansion [26] is 5.10 g/cm^3. Therefore, the number of oxygen sites in chromia per 1 cm^3 can be calculated as follows.

$$N(O\ site) = n \times N_A \times \frac{\rho_{Cr_2O_3}}{M(Cr_2O_3)} = 3 \times 6.02 \times 10^{23} \times \frac{5.10}{151.99}$$

$$= 6.06 \times 10^{22} \text{ cm}^{-3}$$

Where n is the number of oxygen sites in Cr_2O_3, N_A is Avogadro constant, $\rho_{Cr_2O_3}$ is the density of Cr_2O_3 at 800 ºC, and $M(Cr_2O_3)$ is the molar mass of Cr_2O_3.

The ratio of concentration values m easured in the Base specimen and MoP1 specimen to the total oxygen site is 0.113% and 0.034%, respectively. Therefore, even adding a very small amount of Mo of 0.1 wt% (0.06 at.%) can be sufficiently effective. The above calculation results are summarized in Table 1.

Table 1. Summarized calculation results on the oxide ion vacancy

	Diffusion coefficient (cm^2/s)	Concentration (cm^{-3})	Ratio to the total oxygen site (%)
Base	1.78×10^{-12}	6.82×10^{19}	0.113
MoP1	1.24×10^{-12}	2.08×10^{19}	0.034

Through this study, it was found that the concentration of oxide ion vacancy was greatly reduced by the addition of Mo. This decrease in vacancy concentration seems to be the cause of reduction in the diffusion rate of oxygen, which leads to the decrease in the oxidation rate and inhibition of Cr-Mn spinel formation in the innermost part of the oxide scale by oxygen inward diffusion [5].

4. Conclusions

To investigate the effect of Mo addition on the concentration and diffusion coefficient of oxide ion vacancy in the oxide scale formed on Fe-22Cr-0.5Mn ferritic stainless steels at 800 ºC, electrochemical polarization method was employed. After the pre-oxidation for 100 h in ambient air at 800 ºC, the oxide

scale on one side was completely removed and Pt mesh was attached. On the side where the oxide scale remained, 8YSZ plate is placed. And Pt mesh was attached on the top of the 8YSZ plate. The change in electrical current was measured during applying electrical potential through Pt wires welded to Pt meshes. The concentration and diffusion coefficient of oxide ion vacancy were calculated using log (current) versus time curves and solution of the diffusion equation.

The diffusion coefficient and concentration of oxide ion vacancy in the Base specimen were measured as 1.78×10^{-12} cm^2/s and 6.82×10^{19} cm^{-3}, respectively. The diffusion coefficient and concentration of oxide ion vacancy in the MoP1 specimen, which has 0.1 wt% Mo, were measured as 1.24×10^{-12} cm^2/s and 2.08×10^{19} cm^{-3}, respectively. Compared to the specimen without Mo, the diffusion coefficient and concentration of oxide ion vacancy decreased by 30% and 70% in the specimen with Mo, respectively. The oxide ion vacancy concentration of the oxide scale significantly decreased by the addition of Mo. This decrease in vacancy concentration is responsible for a decrease in the diffusion rate of oxygen, which reduces the oxidation rate and inhibits the formation of Cr-Mn spinel in the innermost part of the oxide scale.

Acknowledgements

This research was supported by grants from the Energy Technology Development Project (20203030030020) funded by the Ministry of Trade, Industry and Energy, Republic of Korea.

References

1. S. H. Kim, J. Y. Huh, J. H. Jun, D. H. Kim and J. H. Jun, Evaluation of STS 430 and STS 444 for SOFC Interconnect Applications, *Corrosion Science and Technology*, **6**, 1 (2007). https://www.j-cst.org/data/issue/CST/C000601/C00060100001.pdf
2. S. P. Jiang, J. P. Zhang, and K. Foger, Deposition of Chromium Species at Sr-Doped $LaMnO_3$ Electrodes in Solid Oxide Fuel Cells. II. Effect on O_2 Reduction Reaction, *Journal of Electrochemical Society*, **147**, 3195 (2000). Doi: https://doi.org/10.1149/1.1393883
3. Z. Yang, K. S. Weil, D. M. Paxton, and J. W. Stevenson, Selection and Evaluation of Heat-Resistant Alloys for SOFC Interconnect Applications, *Journal of Electrochemical Society*, **150**, A1188 (2003). Doi: https://doi.org/10.1149/1.1595659
4. H. Yokokawa, H. Tu, B. Iwanschitz, and A. Mai, Fundamental Mechanisms Limiting Solid Oxide Fuel Cell Durability, *Journal of Power Sources*, **182**, 400 (2008). Doi: https://doi.org/10.1016/j.jpowsour.2008.02.016
5. D. W. Yun, H. S. Seo, J. H. Jun, J. M. Lee, and K. Y. Kim, Molybdenum Effect on Oxidation Resistance and Electric Conduction of Ferritic Stainless Steel for SOFC Interconnect, *International Journal of Hydrogen Energy*, **37**, 10328 (2012). Doi: https://doi.org/10.1016/j.ijhydene.2012.04.013
6. D. W. Yun, H. S. Seo, J. H. Jun, and K. Y. Kim, Evaluation of Nb- or Mo-Alloyed Ferritic Stainless Steel as SOFC Interconnect by Using Button Cells, *International Journal of Hydrogen Energy*, **38**, 1560 (2013). Doi: https://doi.org/10.1016/j.ijhydene.2012.11.028
7. S. Kondo, Y. W. Chai, K. Kanai, D.S. Lee, M. Watanabe, S. Ishikawa, T. Yamasita, and Y. Kimura, Intermetallic Phase Precipitation and Oxidation Behavior of Fe–20Cr–0.5Nb–2Mo (at.%) High-Cr Ferritic Alloy at High Temperatures, *Acta Materialia*, **246**, 118677 (2023). Doi: https://doi.org/10.1016/j.actamat.2023.118677
8. B. Hua, J. Pu, F. Lu, J. Zhang, B. Chi, and L. Jian, Development of a Fe–Cr Alloy for Interconnect Application in Intermediate Temperature Solid Oxide Fuel Cells, *Journal of Power Sources*, **195**, 2782 (2010). Doi: https://doi.org/10.1016/j.jpowsour.2009.08.077
9. L. Garcia-Fresnillo, L. Niewolak, W. J. Quadakkers, and G. H. Meier, Influence of Alloying Elements on the Behavior of Different Ferritic Steels as Candidate Materials for SOFC Interconnect, *Oxidation of Metals*, **89**, 61 (2018). Doi: https://doi.org/10.1007/s11085-017-9777-6
10. H. S. Seo, D. W. Yun, and K. Y. Kim, Effect of Ti Addition on the Electric and Ionic Property of the Oxide Scale Formed on the Ferritic Stainless Steel for SOFC Interconnect, *International Journal of Hydrogen Energy*, **37**, 16151 (2012). Doi: https://doi.org/10.1016/j.ijhydene.2012.08.073
11. H. S. Seo, D. W. Yun, and K. Y. Kim, Oxidation Behavior of Ferritic Stainless Steel Containing Nb, Nb–Si and Nb–Ti for SOFC Interconnect, *International Journal of Hydrogen Energy*, **38**, 2432 (2013). Doi: https://doi.org/10.1016/j.ijhydene.2012.12.073
12. L. Niewolak, J. Zurek, E. Wessel, H. Hattendorf, and W.J. Quadakkers, Temperature Dependence of Phase Composition in W and Si-Alloyed High Chromium Ferritic Steels for SOFC Interconnect Applications, *Journal*

of Alloys and Compounds, **717**, 240 (2017). Doi: https://doi.org/10.1016/j.jallcom.2017.05.113

13. B. Kuhn, C. Asensio Jimenez, L. Niewolak, T. Hüttel, T. Beck, H. Hattendorf, L. Singheiser, and W.J. Quadakkers, Effect of Laves Phase Strengthening on the Mechanical Properties of High Cr Ferritic Steels for Solid Oxide Fuel Cell Interconnect Application, *Materials Science and Engineering: A*, **528**, 5888 (2011). Doi: https://doi.org/10.1016/j.msea.2011.03.112
14. T. Thublaor and S. Chandra-ambhorn, High Temperature Oxidation and Chromium Volatilisation of AISI 430 Stainless Steel Coated by Mn-Co and Mn-Co-Cu Oxides for SOFC Interconnect Application, *Corrosion Science*, **174**, 108802 (2020). Doi: https://doi.org/10.1016/j.corsci.2020.108802
15. F. Saeidpour and H. Ebrahimifar, Effect of Nanostructure Fe-Ni-Co Spinel Oxides/Y_2O_3 Coatings on the High-Temperature Oxidation Behavior of Crofer 22 APU Stainless Steel Interconnect, *Corrosion Science*, **182**, 109280 (2021). Doi: https://doi.org/10.1016/j.corsci.2021.109280
16. S. U. Oh, D. K. Kim, I. T. Lee, C. S. Choi, J. A. Lee, Y. W. Heo, and J. H. Lee, Electrophoretic Deposition and Low-Temperature Densification of $Cu_{1.35}Mn_{1.65}O_4$ Spinel for an Interconnect Protective Coating in Solid Oxide Fuel Cells, *International Journal of Hydrogen Energy*, **47**, 33410 (2022). Doi: https://doi.org/10.1016/j.ijhydene.2022.07.259
17. Y. S. Kim, Synergistic Effect of Nitrogen and Molybdenum on Localized Corrosion of Stainless Steels, *Corrosion Science and Technology*, **9**, 20 (2010). https://www.j-cst.org/opensource/pdfjs/web/pdf_viewer.htm?code=C00090100020
18. E. L. Roy, E. A. Cho, H. S. Kim, and H. S. Kwon, Effects of Mo on the Structure and Semiconducting Properties of Passive Film Formed on 18Cr-8Ni Stainless Steels, *Corrosion Science and Technology*, **1**, 432 (2002). https://www.j-cst.org/opensource/pdfjs/web/pdf_viewer.htm?code=C00010600432
19. K. Kanki, K. Nishihara, M. Sagara, and H. Amaya, Effect of Mo Addition on Passive Film of Martensitic Stainless Steels by Semiconductor Analysis in H_2S-CO_2 Environment, *Corrosion*, **79**, 570 (2023). Doi: https://doi.org/10.5006/4190
20. H. Liu, M. M. Stack, and S. B. Lyon, Reactive Element Effects on the Ionic Transport Processes in Cr_2O_3 Scales, *Solid State Ionics*, **109**, 247 (1998). Doi: https://doi.org/10.1016/S0167-2738(98)00101-5
21. A. C. S. Sabioni, R. P. B. Ramos, V. Ji, F. Jomard, W. A. de A. Macedo, P. L. Gastelois, and V. B. Trindade, About the Role of Chromium and Oxygen Ion Diffusion on the Growth Mechanism of Oxidation Films of the AISI 304 Austenitic Stainless Steel, *Oxidation of Metals*, **78**, 211 (2012). Doi: https://doi.org/10.1007/s11085-012-9301-y
22. A. C. S. Sabioni, R. P. B. Ramos, J. Vincent, and F. Jomard, Oxygen Diffusion Study in Oxidation Films of the AISI 304 Austenitic Stainless Steel, *Defect and Diffusion Forum*, **323-325**, 345 (2012). Doi: https://doi.org/10.4028/www.scientific.net/DDF.323-325.345
23. S. Chevalier, G. Strehl, J. Favergeon, F. Desserey, S. Weber, O. Heintz, G. Borchardt, and J. P. Larpin, Use of Oxygen Isotope to Study the Transport Mechanism during High Temperature Oxide Scale Growth, *Materials at High Temperatures*, **20**, 253 (2003). Doi: https://doi.org/10.1179/mht.2003.029
24. L. Marchetti, S. Perrin, O. Raquet, and M. Pijolat, Corrosion Mechanisms of Ni-Base Alloys in Pressurized Water Reactor Primary Conditions, *Materials Science Forum*, **595-598**, 529 (2008). Doi: https://doi.org/10.4028/www.scientific.net/MSF.595-598.529
25. I. Roy, P. K. Ray, and G. Balasubramanian, Diffusion of Multi-Principal Elements Through Stable Cr_2O_3 and Al_2O_3 Scales, *Materialia*, **24**, 101497 (2022). Doi: https://doi.org/10.1016/j.mtla.2022.101497
26. A. M. Dymshits, P. I. Dorogokupets, I. S. Sharygin, K. D. Litasov, A. Shatskiy, S. V. Rashchenko, E. Ohtani, A. Suzuki, and Y. Higo, Thermoelastic Properties of Chromium Oxide Cr_2O_3 (Eskolaite) at High Pressures and Temperatures, *Physics and Chemistry of Minerals*, **43**, 447 (2016). Doi: https://doi.org/10.1007/s00269-016-0808-7